THE JOURNAL OF BIOLOGICAL CHEMISTRY VOL. 286, NO. 21, pp. 18938–18948, May 27, 2011

DNA Binding Restricts the Intrinsic Conformational Flexibility of Methyl CpG Binding Protein 2 (MeCP2)*[S]

Received for publication, February 24, 2011, and in revised form, March 29, 2011 Published, JBC Papers in Press, April 4, 2011, DOI 10.1074/jbc.M111.234609

Jeffrey C. Hansen[‡1], Brian B. Wexler[§2], Danielle J. Rogers[§], Kristopher C. Hite[‡], Tanya Panchenko[§¶], Sandya Ajith[§‖], and Ben E. Black[§¶‖3]

From the [‡]Department of Biochemistry and Molecular Biology, Colorado State University, Fort Collins, Colorado 80523-1870, the [§]Department of Biochemistry and Biophysics, [¶]Graduate Group in Cell and Molecular Biology, and [‖]Graduate Group in Biochemistry and Molecular Biophysics, University of Pennsylvania School of Medicine, Philadelphia, Pennsylvania 19104-6059

Mass spectrometry-based hydrogen/deuterium exchange (H/DX) has been used to define the polypeptide backbone dynamics of full-length methyl CpG binding protein 2 (MeCP2) when free in solution and when bound to unmethylated and methylated DNA. Essentially the entire MeCP2 polypeptide chain underwent H/DX at rates faster than could be measured (*i.e.* complete exchange in ≤10 s), with the exception of the methyl DNA binding domain (MBD). Even the H/DX of the MBD was rapid compared with that of a typical globular protein. Thus, there is no single tertiary structure of MeCP2. Rather, the full-length protein rapidly samples many different conformations when free in solution. When MeCP2 binds to unmethylated DNA, H/DX is slowed several orders of magnitude throughout the MBD. Binding of MeCP2 to methylated DNA led to additional minor H/DX protection, and only locally within the N-terminal portion of the MBD. H/DX also was used to examine the structural dynamics of the isolated MBD carrying three frequent mutations associated with Rett syndrome. The effects of the mutations ranged from very little (R106W) to a substantial increase in conformational sampling (F155S). Our H/DX results have yielded fine resolution mapping of the structure of full-length MeCP2 in the absence and presence of DNA, provided a biochemical basis for understanding MeCP2 function in normal cells, and predicted potential approaches for the treatment of a subset of RTT cases caused by point mutations that destabilize the MBD.

Methyl CpG binding protein 2 (MeCP2) is named for its ability to selectively bind to methylated CpG dinucleotides (1), acting through its methyl DNA binding domain (MBD)[4] (2). MeCP2 is a 53-kDa nuclear protein that is present in high amounts in neuronal tissues, where its stoichiometry approaches one MeCP2 per nucleosome throughout the genome (3). In addition to binding unmethylated and methylated DNA (Refs. 4–6, reviewed in Ref. 7), chromatin (4, 7–9), and RNA (10), MeCP2 interacts with many different nuclear proteins, including Sin3a (11), SUV39H1 (12), HP1 (13), DNMT1 (14), Ski and N-COR (15), PU.1 (16), BRM (17), and ATRX (18). Although originally hypothesized to be a specific repressor of methylated genes (11), MeCP2 is now recognized to be multifunctional, with roles in transcriptional activation and repression (19), RNA processing (20), and chromatin organization (8, 3, 21) (reviewed in Ref. 22). Consistent with these results, MeCP2 is localized to both promoter and intergenic regions in the nuclei of neuronal cells (21). Of note, mutations located throughout the entire length of the MeCP2 amino acid sequence are associated with Rett syndrome (RTT), a severe X-linked neurodevelopmental disorder that afflicts about one in 10,000 girls (23, 24). MeCP2 dysfunction is also involved in autism spectrum disorders (25, 26) and certain cancers (27, 28). Hence, it is important to understand the structure/function relationships that apply to MeCP2 in both the health and disease states.

Intrinsically disordered proteins lack a well folded traditional tertiary structure over some or all of their polypeptide sequence (29–33). Several biophysical techniques that measure averaged solution behavior have recently documented that MeCP2 is an intrinsically disordered protein. Steady-state circular dichroism (CD) measurements revealed that MeCP2 in solution is ~60% unstructured, 35% β-strand/turn, and 5% α-helix (34, 35). Sedimentation equilibrium studies showed that free MeCP2 is a monomer over a wide concentration range, and sedimentation velocity analysis yielded a sedimentation coefficient of 2.2 S (34). Taken together, the analytical ultracentrifugation results demonstrated that MeCP2 has a frictional coefficient that would be expected for a random coil-like molecule. Thus, one can infer from these averaged data that considerable portions of the MeCP2 polypeptide chain lack a secondary structure. However, although the atomic structure of the isolated MBD fragment has been solved alone (36) and in complex with methylated DNA (37), there is no fine resolution structural information available for full-length MeCP2 because of its highly disordered nature, either when free in solution or when bound to DNA.

* This work was supported, in whole or in part, by National Institutes of Health Grants to GM66834 (to J. C. H.), GM82989 (to B. E. B.), and GM08275 (University of Pennsylvania Structural Biology Training Grant) (to T. P.). This work is also supported by a career award in the biomedical sciences from the Burroughs Wellcome Fund and a Rita Allen Foundation scholar award (to B. E. B.).

[S] The on-line version of this article (available at http://www.jbc.org) contains supplemental Figs. S1–S14.

[1] To whom correspondence may be addressed. E-mail: jeffrey.c.hansen@colostate.edu.

[2] Present address: Robert Wood Johnson Medical School, New Brunswick, NJ 08901.

[3] To whom correspondence may be addressed. E-mail: blackbe@mail.med.upenn.edu.

[4] The abbreviations used are: MBD, methyl DNA binding domain; RTT, Rett syndrome; CD, circular dichroism; H/DX, hydrogen/deuterium exchange.

Mass-spectrometry-based hydrogen/deuterium exchange (H/DX) has emerged as a powerful technique for studying the structure of monomeric intrinsically disordered proteins and their higher-order complexes at high resolution. For instance, the dramatic reduction of H/DX rates along the polypeptide backbone of amyloid forming proteins has been characterized at amino acid resolution following their assembly into amyloid (38, 39). For full-length MeCP2, H/DX has the promise to substantially extend the averaged biophysical measurements by providing fine resolution mapping data that locates regions of secondary structure throughout the protein sequence.

In this study, we apply H/DX to the analysis of full-length MeCP2 when free in solution and when bound to unmethylated and methylated DNA. Results demonstrate that the MBD is the only domain within free MeCP2 that shows even modest protection from H/DX, and even the H/DX of the MBD is fast compared with a typical globular protein. This indicates that full-length MeCP2 rapidly samples many different conformational states and tertiary structures when free in solution. We further show that binding of MeCP2 to unmethylated DNA substantially decreases the global conformational flexibility of the MBD, whereas the rapid H/DX exchange elsewhere in the protein was unaffected. Thus, even with the increased H/DX protection in the MBD, full-length MeCP2 remains a very intrinsically disordered protein when bound to DNA. Relative to binding to unmethylated DNA, binding to methylated DNA only slightly increases the conformational rigidity in a local region within the N-terminal portion of the MBD. Finally, we examine the effects of several common RTT mutants on the properties of the isolated MBD, and find widely varied effects. Taken together, the H/DX experiments yielded high-resolution structural dynamics data characterizing the extreme intrinsic conformational flexibility of full-length MeCP2 and also provided accompanying information about how the structure and stability of the MeCP2 MBD is affected by DNA binding and certain specific RTT mutations. For the latter case, the implications for treatment of RTT are discussed.

EXPERIMENTAL PROCEDURES

Protein Expression and Purification—Full-length human MeCP2 isoform e2 and the isolated WT and R106W, F155S, and T158M mutant MBD polypeptides were purified using a modification of the protocol described previously (34). Recombinant proteins were expressed using the IMPACT system (New England Biolabs). Constructs were subcloned into the ptyb1 plasmid vector. MBD mutant constructs were kindly supplied by Dr. C. L. Woodcock. All purified proteins contained a vestigial sequence, EFLEGSSC, on their C-terminal ends as a result of cloning methods described previously (34). *Escherichia coli* BL21RP+ was used as host expression bacteria grown in lysogeny broth at 37 °C to an optical density of 0.5 absorbance unit, induced with 0.4 mM isopropyl 1-thio-β-D-galactopyranoside and cooled to 18 °C for 2–3 h prior to harvest. Expression hosts were pelleted in an Avanti J-26 XPI preparative centrifuge (Beckman Coulter) in a JLA-8.100 rotor at 5,000 × *g* for 15 min. Pellets were resuspended in wash buffer (25 mM Tris (pH 7.5), 100 mM NaCl) and repelleted under the same conditions. Clean pellets were resuspended in column buffer (25 mM Tris-HCl (pH 8.0), 500 mM NaCl) supplemented with 0.1% Triton X-100, 0.2 mM PMSF, and Protease Inhibitor Mixture Set II (Calbiochem), followed by two rounds of sonication, 90 s each, using a Branson Sonifier 450 with a large tip at 50% duty cycle and a power output of 7. The lysate was transferred to Oakridge tubes and spun at 21,000 × *g* for 25 min in the preparative centrifuge in a JA-17 rotor (Beckman Coulter). The supernatant was bound overnight to chitin beads (New England Biolabs) previously equilibrated in column buffer. Chitin beads were washed with five column volumes of column buffer, decanted, and washed with an equal volume of column buffer supplemented with NaCl to 900 mM NaCl final concentration to wash off errant bacterial DNA left from sonication. The chitin beads were washed with an additional 5 column volumes of 500 mM NaCl column buffer. Chitin binding protein-MeCP2 chimeras were cleaved on the column (40). Column buffer supplemented with 50 mM DTT was passed through the column so that 1 cm of buffer remained between the top of the column bed and the meniscus in a 10-cm Kontes FlexColumn (Fisher) and left for 48–72 h for complete cleavage. Protein was eluted from the chitin column with column buffer, diluted from 500 mM to 300 mM NaCl, and loaded onto a HiTrap Heparin HP column (GE Healthcare). Proteins were eluted from the heparin column via step gradient from 300 mM NaCl to 1 M NaCl buffer using 100 mM NaCl steps in 25 mM Tris (pH 7.5), 10% glycerol background buffer. Peak fractions were pooled and dialyzed into 10 mM Tris (pH 7.5).

Formation of MeCP2-DNA Complexes—Unmethylated and methylated 198-bp DNA fragments derived from the sea urchin 5S rRNA gene were prepared as described (34). This DNA has 12 methylatable CpGs. Purified MeCP2 (155 μl, 0.80 mg/ml) was added to either an unmethylated or methylated 198-bp DNA fragment (430 μl, 0.2 mg/ml) in a total of 585 μl of 10 mM Tris (pH 7.5), 10 mM NaCl buffer. MeCP2 minimally binds 11 bp of DNA (9). Under these conditions, unmethylated and methylated DNA binding sites were present in molar excess over MeCP2, and DNA concentrations were always above the K_d (5) so that H/DX was being measured under saturated binding conditions and dual population (*i.e.* bound and unbound to DNA) affects were avoided.

H/DX Reactions—A total of 10 μl of each sample (4–10 μg full-length MeCP2 (alone or in a complex with the indicated DNA fragment) or 0.4–3 μg of MBD fragments (the wild-type version or indicated RTT-associated mutation)) was mixed with 30 μl of D_2O containing 10 mM Tris (pH 7.2), 10 mM NaCl and incubated at the indicated temperature. At each indicated time point, the H/DX samples were added to vials containing 60 μl of a quench solution (0.8 M guanidinium-HCl, 0.8% formic acid, 10% glycerol) at 0 °C and immediately frozen in liquid N_2. The samples were stored at −80 °C until analysis by MS.

Protein Fragmentation and MS—H/DX samples were individually melted at 0 °C and then injected (100 μl) and pumped through tandem immobilized protease (pepsin and fungal protease XIII, both from Sigma) columns (50 μl/min, 1 × 20 mm (16 μl) columns of each protease coupled to Poros 20 AL support (Applied Biosystems)). Protease-generated fragments were collected onto a C18 HPLC trap column (2.5 × 0.5 mm). Peptides were eluted into and through an analytical C18 HPLC

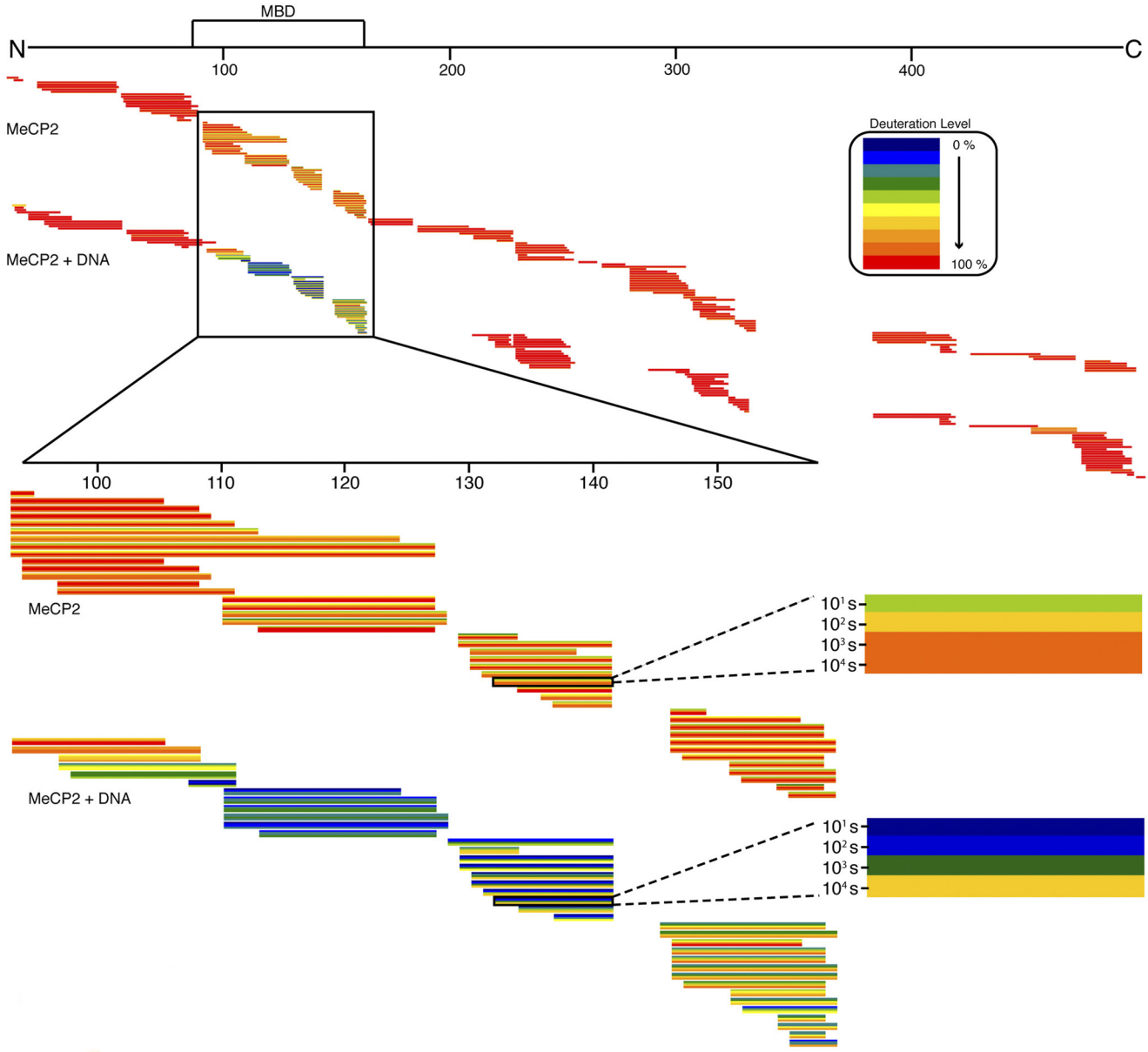

FIGURE 1. **Protection from H/DX before and after DNA binding is detectable only within the MBD of MeCP2.** Each *horizontal bar* represents an individual peptide derived from MeCP2 when free in solution (*MeCP2*), or bound to unmethylated DNA (*MeCP2 + DNA*). The *peptide bars* are color-coded for the percent deuteration at 4 °C at each time point (10^1, 10^2, 10^3, and 10^4 s), as represented by an individual stripe within each bar. The MBD is enlarged on the lower left side, with an individual peptide enlarged further and labeled to illustrate the inclusion of each time point for every peptide in the data set.

column (0.3 × 75 mm) by an acetonitrile gradient (12–55% B; 6 μl/min; solvent A, 0.1% formic acid; solvent B, 0.1% formic acid, 99.9% acetonitrile), and the effluent was directed to the mass spectrometer (LTQ Orbitrap XL, Thermo Fisher Scientific). The SEQUEST software program (Thermo Fisher Scientific) was used to identify the likely sequence of the parent peptides using non-deuterated samples via tandem MS.

H/DX Analysis—DXMS software (Sierra Analytics) was used for searching the MS1 data from H/DX samples and calculating the centroid of the isotopic envelope of each peptide using a general scheme that is described elsewhere (41, 42). Peptides that scored highly in the DXMS program were checked for matching of calculated *versus* known mass, charge state, and the retention time of the peptide on the C18 column, and peptides that satisfied these criteria were selected for further analysis. The level of H/DX occurring at each time point is expressed as either the number of deuterons or the percentage of exchange within each peptide. In each case, corrections for loss of deuterium label by individual peptides during H/DX-MS analysis were made through measurement of loss of deuterium from reference samples that had been deuterated under denaturing conditions as described elsewhere (43, 44). Maps of rate-classes along the polypeptide sequence were assembled using the H/DX data as described (41, 45).

RESULTS

We first used H/DX to analyze the polypeptide backbone dynamics of full-length MeCP2 when free in solution (Fig. 1). Because MeCP2 binds strongly to unmethylated and methylated DNA (7), we also determined the dynamics of H/DX when

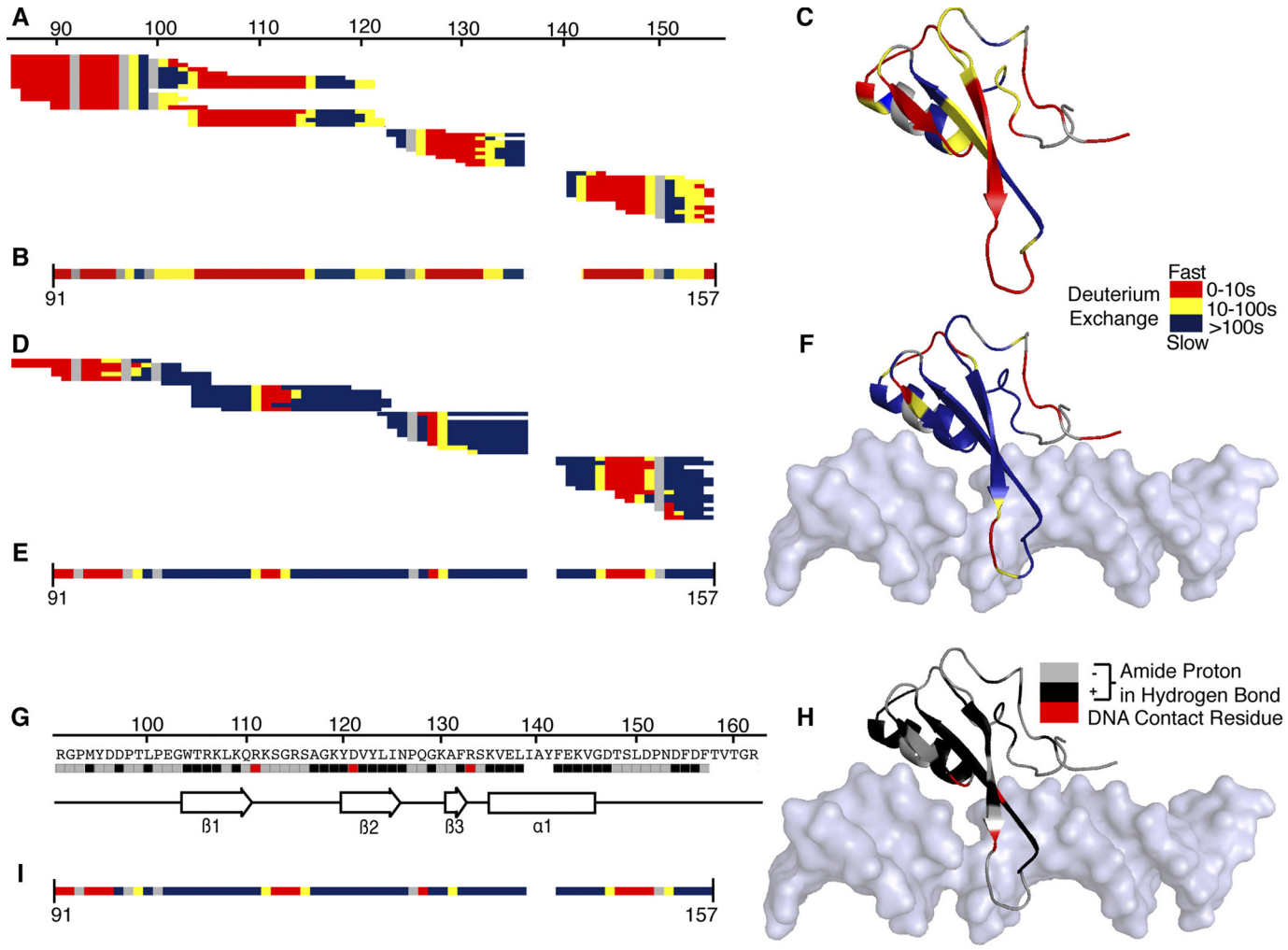

FIGURE 2. **Stabilization of the MBD upon unmethylated DNA binding results from restricted sampling of intrinsic unfolding rates.** *A*, deuterium exchange profile maps for each peptide of the MBD of free MeCP2 in solution. *B*, the consensus exchange rate at each position from *panel A* is shown in a single linear representation. The data shown span from residue 91, the N-terminal residue of the MBD clear in the crystal structure (37), to residue 157, the C-terminal residue where our high-density coverage of the MBD ends. *C*, the consensus map from *B* overlaid onto the crystal structure of the MBD (the DNA is not shown, PDB code 3C2I). *D*, the exchanged deuterons for each MBD peptide bound to unmethylated DNA, mapped as in *A*. *E*, the consensus map of *D*. *F*, the consensus map from *D* overlaid onto the crystal structure of the MBD. *G*, the MBD sequence with the location of residues where the amide proton is engaged in a hydrogen bond in the crystal structure (*black*), as well as the position of the reported residues (37) with direct DNA contacts (*red*). *H*, mapping of the residue labeling from *G* onto the MBD crystal structure. *I*, a structure-biased consensus map using the same number of slow (*blue*), medium (*yellow*), and fast (*red*) exchanging amino acid position as in *E*. Note how closely the slow (*blue*) residues in the final consensus map match amide proton protection predicted by the stable structure obtained by others by crystallography (37). This indicates that the increase in protection upon binding to unmethylated DNA result from stabilizing the overall fold of the MBD rather than increasing protection locally at its relatively small DNA binding surface.

MeCP2 was bound to an unmethylated 198-bp DNA fragment derived from the sea urchin 5S rRNA gene (34) (Figs. 1 and 2 and supplemental Figs. 1–4) and to the methylated version of the same DNA fragment (Figs. 3 and 4 and supplemental Figs. 5, 7–9). In Figs. 2–4, the H/DX experiments characterize full-length MeCP2, focusing on the MBD region of the protein.

H/DX Demonstrates the Extreme Conformational Plasticity of Full-length MeCP2 When Free and Bound to DNA—The H/DX approach consisted of incubation of the samples in heavy water (D_2O) at 4 °C to exchange deuterium with the amide protons along the polypeptide backbone of MeCP2. At time points spanning 10^1 s to 10^4 s, the exchange reactions were quenched, MeCP2 fragmented by proteolysis, and deuterium incorporation measured by mass spectrometry. Protection from H/DX in native proteins or protein-DNA complexes is expected in those regions that are folded into stable secondary structures. This is due to the fact that measurable amide protons are hydrogen-bonded and must transiently lose secondary structure, locally or globally, for exchange to occur (39).

In our experiments, peptides covering 87% (free MeCP2) or 73% (MeCP2 bound to unmethylated DNA) of the entire length of the MeCP2 sequence were initially identified by MS/MS and then successfully monitored over the entire time course of exchange. In the absence of DNA, H/DX along nearly the entire length of MeCP2 was rapid, with 64% of all peptides measuring >90% of complete exchange by the first time point (10 s). The sole region that exhibited measurable protection from H/DX was found in the peptides approximately spanning amino acids 90–160, closely overlapping the MBD of MeCP2 (which encompasses residues 78–162). These results indicate that when free in solution, full-length MeCP2 has only one region of even marginally stable secondary structure,

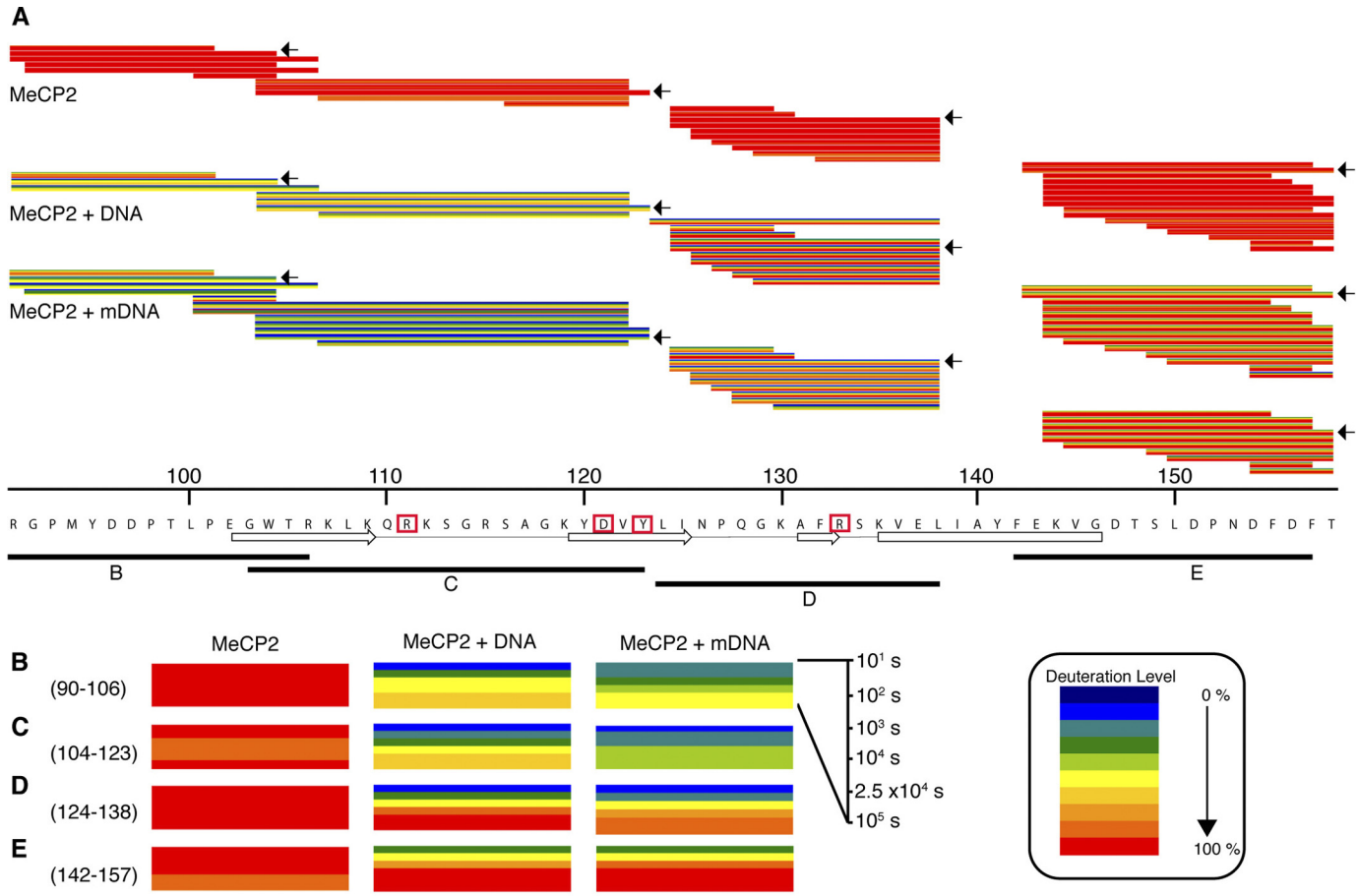

FIGURE 3. **Binding to methylated DNA further increases protection from H/DX within the N-terminal but not the C-terminal portion of the MBD.** *A*, peptides from the MBD are shown for free MeCP2 (*top panel*), MeCP2 bound to unmethylated DNA (*center panel*), and MeCP2 bound to methylated DNA (*bottom panel*). Data are presented as in Fig. 1. *B–E*, representative peptides that span the MBD with the indicated amino acid positions are enlarged and compared. The residues boxed in *red* indicate positions that directly contact DNA and/or form bonds with water molecules that are coordinated with the methyl groups on methylated DNA.

corresponding to the MBD. Besides the MBD, our findings indicate that the remainder of free full-length MeCP2 lacks an ordered structure.

When bound to unmethylated DNA under saturating conditions, the MBD-derived peptides were much slower to exchange, whereas there was no change observed in the very rapid H/DX at any other location in the MeCP2 protein sequence (Fig. 1 and supplemental Fig. 1). Thus, although the stability of the MBD was greatly increased when MeCP2 was bound to unmethylated DNA, the remainder of the polypeptide chain stayed extremely disordered. The MBD only accounts for 17% of the 486-residue full-length protein. Thus, the data in Fig. 1 demonstrate that MeCP2 remains mostly disordered, even when bound to DNA. Given that the MBD was the sole region to show evidence of secondary structure formation, we focused our next experiments on high-resolution H/DX characterization of the dynamics of the MBD in full-length MeCP2 when free and bound to DNA.

Rapid Sampling of Partially Unfolded States Occurs within the MBD When MeCP2 Is Free in Solution—Because the MBD region was particularly well represented with many partially overlapping peptides, we could employ an H/DX rate mapping strategy that has been especially informative in other studies when combined with available crystal structures (45, 46). In the absence of DNA, only small regions (*i.e.* stretches of one to four amino acids, *blue* positions in Fig. 2, *A* and *B*) exchange amide protons for deuterons slower than 100 s. Thus, the stability at many locations within the MBD is the same or only marginally greater than the remainder of the MeCP2 polypeptide chain when the protein is free in solution. Further, when the H/DX profile of the MBD of free MeCP2 is mapped (Fig. 2*C*) onto the crystal structure of the MBD (37), it is clear that even in the most rigid portion each β-strand and the α-helix in this region must rapidly sample partially unfolded conformations to allow for the relatively rapid H/DX (*i.e.* nearly complete exchange by 1000 s at every location) that is observed in the MBD of the free full-length protein (Fig. 1).

Rapid Sampling of Partially Unfolded States within the MBD Is Restricted When MeCP2 Binds to Unmethylated DNA—MeCP2, when bound to unmethylated DNA under saturating conditions, has many more residues within the MBD that are substantially protected from H/DX (Fig. 2*D*). On the level of individual peptides, whereas exchange is complete by 10^4 s within the MBD of the free protein, when MeCP2 is bound to DNA, several MBD residues remain protected from H/DX at the same 10^4 s time point (supplemental Figs. 2–4).

When we examined the H/DX protection imposed upon the MeCP2 MBD because of unmethylated DNA binding in closer

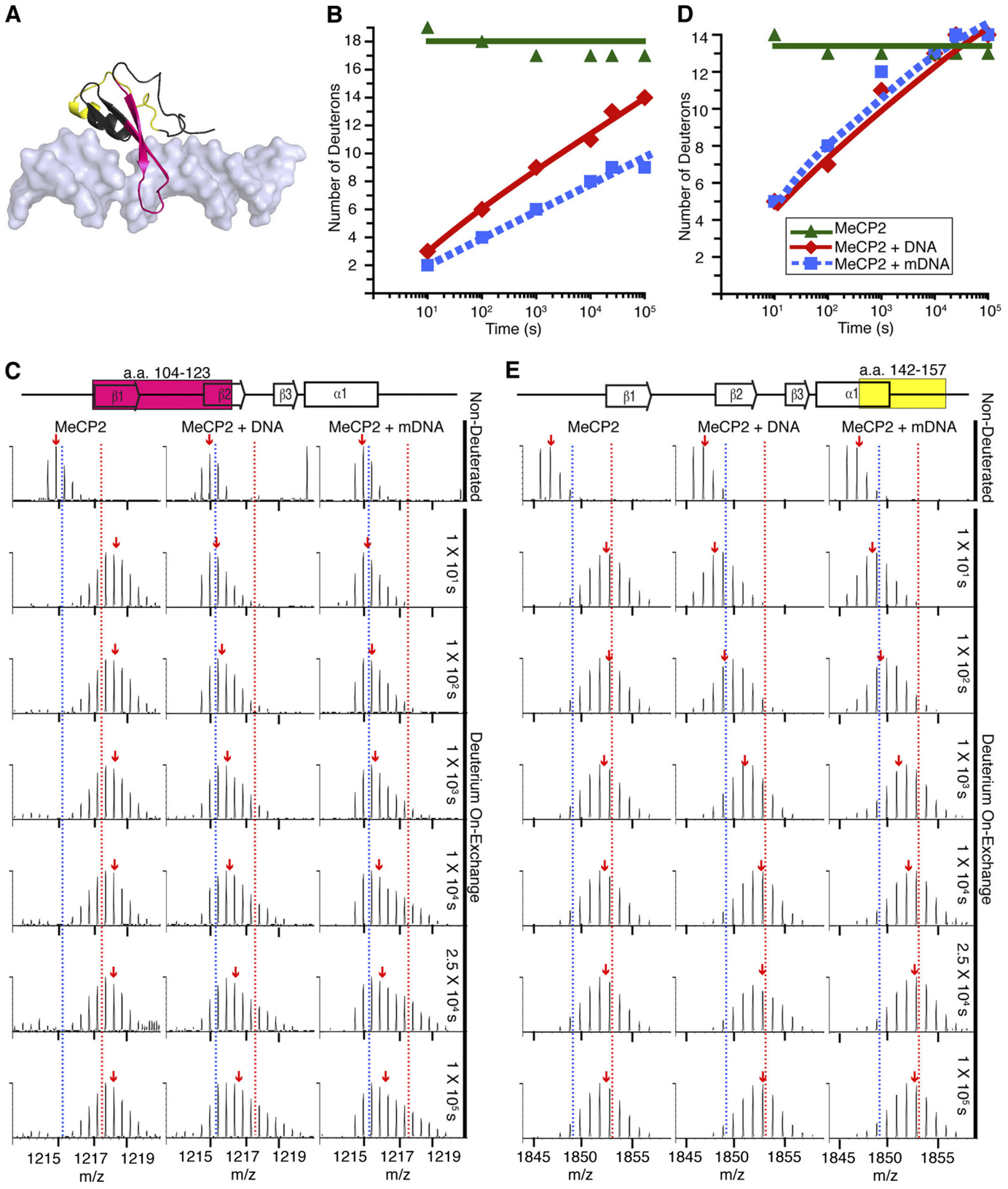

FIGURE 4. **Representative MBD peptides showing protection from H/DX when MeCP2 binds to unmethylated DNA and methylated DNA.** *A*, the location on the crystal structure of the MBD bound to methylated DNA (PDB code 3C2I) of representative MBD peptides (amino acids 104–123 (*pink*) and 142–157 (*yellow*). *B* and *D*, comparison of H/DX for peptides amino acids 104–123 (*B*) and amino acids 142–157 (*D*) from free MeCP2 and MeCP2 bound to unmethylated DNA and methylated DNA. *C* and *E*, side-by-side analysis of raw data for the indicated peptides from free MeCP2 (*left panel*), MeCP2 bound to unmethylated DNA (*center panel*), or MeCP2 bound to methylated DNA (*right panel*). *Dotted blue* and *red* lines are guideposts to highlight the differences in *m/z* shifts reflecting the magnitude of H/DX. *Red arrows* mark the location of the centroid value of the peptide in each case.

detail (Fig. 2*E*), we noted that the H/DX profile closely matched the known secondary structural elements (36, 37) of the isolated MBD (Fig. 2*F*, *blue* residues labeling the most protected regions of MeCP2 when bound to DNA). In the crystal structure of the MBD bound to methylated DNA (37), the majority of the surface of the isolated MBD is exposed to solvent, not buried with the surface of the bound DNA. The amide protons of Arg-111, Asp-121, and Arg-133 (labeled *red* in Fig. 2, *G* and *H*) are the only positions predicted from the crystal structure (37) to become protected by DNA contacts, which cannot explain the extent of protection of H/DX we observed upon unmethylated DNA binding by MeCP2 (compare protection in Fig. 2, *B* and *E*). Our scheme for generating H/DX profiles of the MBD allowed for resolution down to a small number of amino acids (see "Experimental Procedures"). As described above, there is a strong correlation between the H/DX of the MBD of MeCP2 when bound to unmethylated DNA and the secondary structure of the MeCP2-methylated DNA complex (Fig. 2, *E* and *F*). Our H/DX profiles (Fig. 2, *B* and *E*) were generated without bias toward any structural information, but if we include predicted protection (*G* and *H*) in positioning the measured H/DX on each peptide, the final profile (*I*) only differs from the unbiased profile (*E*) at seven positions. This indicates that the slowed backbone exchange upon unmethylated DNA binding corresponds to global stabilization of the same folded secondary structural elements observed in the structural studies of the MBD.

To summarize, our data indicate that the H/DX protection of the MBD upon binding of MeCP2 to unmethylated DNA occurs mainly via domain-wide restriction of rapid sampling of its secondary structural elements, not by inaccessibility to solvent because of steric hindrance imposed by DNA. That is, the increase in H/DX protection upon binding unmethylated DNA is due to stabilization of the overall fold of the MBD rather than increased local protection at its relatively small DNA binding surface. In addition, there are fundamental changes in the flexibility of the MBD structure that occur upon DNA binding that occur even when the DNA is unmethylated.

Binding to Methylated DNA Locally Restricts Conformational Flexibility within the MBD—Given that MeCP2 only has a modest preference for methylated DNA over unmethylated DNA (5), we were curious of the extent to which binding to methylated DNA would correspond to increased H/DX protection within the MBD (or elsewhere in the protein). Our initial experiments (Figs. 1–2) were performed at 4 °C to slow the chemical exchange rate and maximize our ability to see any protection at all for free MeCP2. Because many residues were completely protected from exchange at 10^4 s when MeCP2 was bound to unmethylated DNA at 4 °C (Figs. 1 and 3 and supplemental Figs. 2–5) or 23 °C (supplemental Fig. 5), we predicted that further increasing the temperature would be necessary to perform a reasonable time course that spanned the exchange rates of most of the protected portions of the MBD in the case of DNA-bound (either unmethylated or methylated) MeCP2. To determine whether this was the case, we first analyzed MeCP2 at a single time point at three varied temperatures (4 °C, 23 °C, and 37 °C) and measured H/DX on peptides within the MBD (supplemental Fig. 6). This experiment indicated that increased temperature (most likely corresponding to predictable higher chemical rates of H/DX (39)) increased the amount of H/DX within the MBD. Thus, we chose to perform an expanded time course (1×10^1, 1×10^2, 1×10^3, 1×10^4, 2.5×10^4, and 1×10^5 s time points) of H/DX at 37 °C. With peptide coverage spanning much of the full length of MeCP2 in all three cases (MeCP2 alone, plus unmethylated DNA, and plus methylated DNA supplemental Fig. 7), the only observed region with any measurable protection from H/DX once again was within the MBD (Fig. 3*A*). In the absence of DNA, all MBD peptides were >90% deuterated at 10 s, with substantial slowing (most greater than 10^3-fold) of exchange for all MBD peptides when MeCP2 was bound to either unmethylated or methylated DNA (Fig. 3*A*).

In the MeCP2-methylated DNA crystal complex (37), structured waters connect the methyl groups on the DNA with specific MBD residues (Arg-111, Asp-121, Tyr-123, and Arg-133) via hydrogen bonding. To test how the conformational flexibility of the MBD is affected by methylated DNA-specific contacts, we carefully examined representative peptides for which we had a comprehensive MS data set for all samples and time points. Peptides approximately spanning the N-terminal half of the MBD, *i.e.* amino acids 90–106 (Fig. 3*B* and supplemental Fig. 8) and amino acids 104–123 (Figs. 3*C* and 4, *A*–*C*), showed a clear reduction in H/DX rates when MeCP2 was bound to methylated *versus* unmethylated DNA, whereas peptides approximately spanning the C-terminal half of the MBD, *i.e.* amino acids 124–138 (Fig. 3*D* and supplemental Fig. 9) and amino acids 142–157 (Figs. 3*E* and 4, *A*, *D*, and *E*), showed little or no alteration. The N-terminal peptides showed additional protection exceeding that which would be expected if the residues were only involved in hydrogen bonding with the structured waters. For instance, none of the residues in the amino acids 90–106 peptide, and only three (Arg-111, Asp-121, and Tyr-123) in the amino acids 104–123 peptide, are directly bonded to the structured waters implicated in methylated DNA specificity, yet several additional amide protons exhibit slowed exchange in a manner that was dependent upon binding to methylated DNA (Fig. 4*B* and supplemental Fig. 8). On the other hand, the third residue (Arg-133) that participates in a hydrogen bond with one of the structured waters appeared to have almost no influence on H/DX exchange within the MBD (see a representative peptide corresponding to amino acids 124–138, supplemental Fig. 9). These results indicate that 1) relative to binding to unmethylated DNA, binding to methylated DNA affects H/DX locally (only approximately the N-terminal half of the MBD) and not globally throughout the entire domain, 2) the additional protection of the N-terminal MBD peptides is consistent with additional local rigidity, not solely backbone protection resulting from the residues directly hydrogen-bonded to the structured waters that are coordinated with the methyl groups on the DNA, and 3) the local added protection from H/DX upon binding to methylated DNA *versus* unmethylated DNA is not due to differences in binding kinetics with the MBD because the C-terminal peptides (approximately spanning amino acids 124–157) exchange with indistinguishable slow kinetics when MeCP2 is bound to either DNA fragment compared with the rapid H/DX when MeCP2 is free in solution.

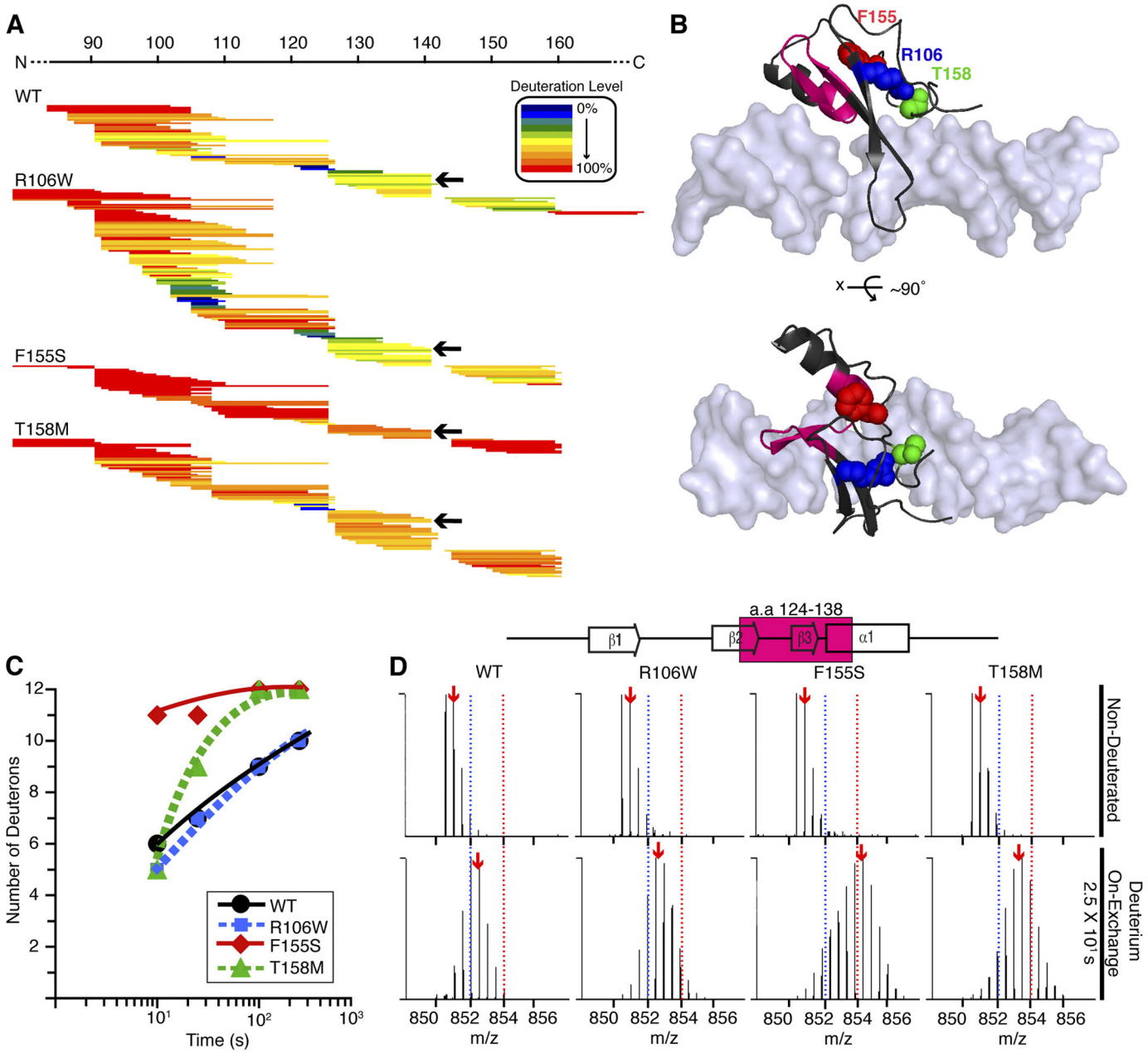

FIGURE 5. **Effects of Rett Syndrome-associated missense mutations on the conformational flexibility of the isolated MBD.** *A*, the levels of H/DX at 2.5 × 10^1 s are color-coded as indicated on *horizontal bars* representing peptides derived from the WT MBD and the MBDs harboring the indicated point mutations. Data from all time points monitored (1 × 10^1, 2.5 × 10^1, 1 × 10^2, and 2.5 × 10^2 s) are shown in supplemental Figs. 10–13. The *black arrows* indicate the representative peptide (amino acids 124–138, compare *C* and *D*, below). *B*, the location on the MBD crystal structure (PDB code 3C2I) of the peptide (amino acids 124–138) highlighted in *C* and *D*. The positions of the amino acid side chains in the RTT MBD mutants that were investigated are shown as colored spheres. *C*, comparison of H/DX for a peptide (amino acids 124–138) from the MBD. *D*, side-by-side analysis of raw data for the WT MBD and the MBDs harboring the indicated mutations. Labeling is as in Fig. 4*C*.

RTT Mutations in the MBD Have Varied Effects on Local and Domain-wide Flexibility—Mutations within the MBD are common in RTT patients, with many of the most frequent missense mutations (such as R106W and T158M) predicted to disrupt stabilizing interactions within the domain (37). For instance, the side chain of Arg-106 forms hydrogen bonds with the polypeptide backbone at positions Thr-158 and Val-159 (37). The extent to which these hydrogen bonds affect dynamic protein behavior is not easily discernable from static structures, but we reasoned that H/DX would provide a fine resolution dynamic measurement to directly assess the local and domain-wide effects of RTT mutations in the MBD (Fig. 5 and supplemental Figs. 10–13). For this analysis, H/DX experiments were performed at 4 °C with isolated MBD peptides bearing specific RTT mutations.

Our results indicate that the R106W MBD mutant had generally similar H/DX behavior as the WT MBD (Fig. 5, *A*, *C*, and *D*), with increased H/DX protection in the β1 peptide and only minor acceleration of exchange occurring in peptides approximately spanning amino acids 140–155 (Fig. 5*A*). By contrast, the F155S mutation, which removes hydrophobicity from within the MBD protein fold (see the position of Phe-155 in Fig.

5*B*) and has been shown previously to greatly destabilize the MBD by fluorescence anisotropy measurements and melting experiments (35), forces the entire MBD to sample unfolded conformations at rates that are several orders of magnitude higher than for the protected residues in the wild-type MBD. Consequently, for the F155S mutant, even at the earliest time point (10 s) there is complete exchange throughout the domain (Fig. 5*C* and supplemental Fig. 12). The side chain of Thr-158 is predicted from the cocrystal structure to be important for the integrity of the so-called Asx-ST motif (located at the C-terminal end of the MBD), in part by making hydrogen bonds with the polypeptide backbone at positions Gly-161 and Arg-162 (37). T158M is the site of the most common point mutation in RTT, accounting for ~9% of all cases. Despite residing in the MBD C terminus, the T158M mutation surprisingly affects conformational dynamics spanning portions well into the N-terminal folded portion of the MBD, approximately including amino acids 125–155 (refer to Fig. 5*D* and the representative peptide (amino acids 124–138) that fits into the major grove of DNA (Fig. 5*B*)). The H/DX behavior of the RTT MBD mutants indicates the variable extent to which these common mutations affect the local and global conformational dynamics of the MBD of MeCP2.

DISCUSSION

Full-length MeCP2 Structure—The structure of full-length MeCP2 is not consistent with a conventional protein comprised of stable, folded domains. Based on averaged biophysical measurements, the conformation of full-length MeCP2 is very disordered, *e.g.* deconvolution of CD data yields 60–65% unstructured content, and the protein sediments as if it were a random coil (34). Prediction algorithms (PONDR-VXT, FoldIndex) also yield estimates of approximately 65% disorder, with short regions of predicted order interspersed throughout an otherwise intrinsically disordered polypeptide chain (34, 47). MeCP2 is composed of six biochemically defined domains: the N-terminal domain, the MBD, the intervening domain, the transcriptional repression domain, and the C-terminal domain α and β (supplemental Fig. 14, 34, 47). CD analysis of the isolated MeCP2 domains indicates that each has between 60–80% unstructured content with the exception of the MBD, and even the MBD is approximately 40% unstructured (47, supplemental Fig. 14). Although the steady-state CD experiments have documented the extensively unstructured nature of full-length MeCP2, they have also raised an important question: Is the 35–40% averaged secondary structure content calculated to be present in MeCP2 and its domains in the form of stable three-dimensional structures, or does it result from rapid sampling of unfolded, random-coil state(s) during the course of the steady-state measurements? Our H/DX experiments indicate that the latter possibility is correct. We obtained nearly total peptide coverage of the MeCP2 polypeptide chain in our experiments, and all domains of MeCP2, except the MBD, underwent essentially complete H/DX at the earliest measureable time point (Fig. 1). Although H/DX was slower in the MBD, in the absence of DNA binding it was still faster than the H/DX of a typical globular protein. Accordingly, we envision that the full-length MeCP2 polypeptide chain rapidly samples many different secondary structures and equilibrates between multiple tertiary structures, even when bound to DNA. In this regard, various domain-domain interactions in *cis* and *trans* have been detected previously (35, 47), consistent with the conformational malleability of full-length MeCP2 observed by H/DX.

What are the functional advantages of the extreme conformational flexibility and fast conformational sampling exhibited by MeCP2? This is a key question, as it is relevant to the subject of intrinsically disordered proteins in general. Given that intrinsically disordered proteins often acquire secondary structure in conjunction with macromolecular interactions (48), we propose that enhanced conformational flexibility and rapid structural sampling 1) provide the biochemical basis of MeCP2 multifunctionality by allowing the 53-kDa monomeric protein to bind to so many different macromolecular partners (11–18), and 2) facilitate the formation of higher-order macromolecular complexes involved in MeCP2 function that themselves are conformationally malleable (see (49)).

MeCP2-DNA Interactions—Very few proteins have been investigated where H/DX has been used to probe the conformational rigidity imposed by binding to DNA. One case is the Lac repressor, which is capable of binding to nonspecific DNA sequences but binds specifically to its operator sequence with $>10^6$-fold higher affinity (50). When bound to DNA nonspecifically, the conformational flexibility of the folded portion of the Lac repressor DNA binding domain is unaffected as measured by H/DX (51). Only upon forming the base-specific hydrogen bonds with its operator sequence (52) is there imposed a substantial (10^5-fold) increase in conformational rigidity throughout the Lac repressor DNA binding domain (51). Another example is the rigidity imposed upon core histones during nucleosome assembly. Subnucleosomal histone complexes, upon assembly into nucleosomes, undergo $>10^3$-fold protection from H/DX, spanning the globular domains of each of the core histones (42). For both Lac repressor and histone H/DX protection upon DNA binding, the effects appear to be global throughout domains (*i.e.* not local at the points directly contacting DNA). Moreover, the H/DX data for these proteins cannot be explained generally by solvent inaccessibility in the bound state, but rather by inflexibility gained in secondary structural elements upon either specific (Lac repressor) or nonspecific (histone) DNA binding.

In the case of MeCP2, we found that global, domain-wide inflexibility is conferred to the MBD upon nonspecific binding to a 198-bp unmethylated DNA fragment. Moreover, binding to the methylated version of the same DNA (containing 12 CpG sites) subsequently leads to additional local protection in the MBD. The global inflexibility gained upon unmethylated DNA binding is substantial, at least 1000-fold slower H/DX at many locations throughout the MBD (Figs. 1 and supplemental Figs. 2–4). Importantly, a clear feature upon comparing the effects on MBD polypeptide backbone dynamics resulting from binding unmethylated or methylated DNA is not the differences in H/DX but the striking similarities. That is, our H/DX experiments strongly suggest that the MBD folds and recognizes double-stranded DNA in a manner that is very similar when it is bound to either unmethylated or methylated DNA. There is somewhat more protection in the N-terminal half of the MBD

when bound to methylated DNA but no measurable differences in the C-terminal half (Figs. 3 and 4 and supplemental Figs. 8 and 9). Thus, we can conclude that in addition to the changes imparted by unmethylated DNA binding, the methyl groups coordinate waters with the MBD in a manner that increases the affinity of the DNA interaction several-fold and increases backbone rigidity in the N-terminal half of the domain, which contains three of the four residues that interact with the structured waters. The NMR solution structures (36) and the crystal structure (37) provide clear views of a favored folded state of the molecule, but to understand the dynamics of unfolding/refolding of the MBD, a measurement that is capable of characterizing dynamic protein behavior, such as the H/DX approach described here, needed to be employed. In this regard, CD analysis has shown that MeCP2 and many of its isolated domains gain secondary structure content when bound to unmethylated and methylated DNA (35, 47). These averaged measurements are likely assaying the same global and local decreases in MBD flexibility observed by H/DX.

Previous studies have demonstrated that the isolated intervening domain, transcriptional regression domain, and C-terminal domain α of MeCP2 are each capable of binding unmethylated DNA in native gel mobility shift assays (47). However, as discussed above, the H/DX experiments find no evidence of protection outside the MBD when MeCP2 is bound to unmethylated DNA. Thus, the intervening domain, transcriptional regression domain, and C-terminal domain α may continue to sample multiple conformational states even as they interact nonspecifically with DNA. MeCP2 is an abundant chromatin-associated protein *in vivo* (3, 53). In terms of chromatin, we speculate that the MBD binds to linker DNA (4, 5, 9), whereas other DNA binding site(s) are used to interact with nucleosomal DNA and help MeCP2 to physically envelop the nucleosome (54). This in turn promotes compaction of MeCP2-bound chromatin fibers (8, 9). In summary, our H/DX experiments allowed us to access site-specific backbone dynamic information that complements the earlier structural studies and significantly extends our understanding of the physical and chemical mechanisms of DNA binding of this highly abundant and functionally important component of neuronal chromatin.

MBD RTT Mutations—The H/DX approach has yielded novel information about the flexibility of several common RTT MBD mutants that cannot be discerned from the static cocrystal structure or averaged solution measurements. All three mutations (R106W, F155S, and T158M) that we chose to study replace side chains that do not directly contact DNA (or waters coordinated by the methyl groups on methylated DNA) but rather were predicted from static models (36, 37) to be important for the structural integrity of the MBD. For example, on the basis of direct hydrogen bonding seen in the crystal structure, the Thr-158 residue was proposed to stabilize the Asx-ST motif in the extreme C-terminal region of the MBD along with residue Arg-106 in the N-terminal portion of the MBD, yet with the T158M mutant the H/DX clearly showed increased flexibility of peptides that span the secondary structural elements (β1 and β2 strands and α2 helix) that lie between the MBD termini (Fig. 5). The R106W mutant is predicted to be disruptive of the Asx-ST motif (37) and potentially disruptive to the integrity of the entire MBD. However, for this mutant, the H/DX was virtually identical to the wild-type MBD, clearly not generating instability that leads to a higher frequency of sampling an unfolded state that is transmitted throughout the domain. Ultimately, the H/DX data suggest that interactions between the N terminus and C terminus of the MBD that are likely to be disrupted by either the T158M or R106W mutations may affect DNA binding, and indeed, this has been demonstrated recently (35). The F155S mutant does not affect any proposed hydrogen bonds with DNA or water-mediated DNA contacts, yet this mutation yields the most rapid conformational sampling of any of the three mutations tested, probably by its disruption of hydrophobic contacts with the many neighboring side chains lining the interior of the MBD fold. As might be expected, this mutant potently disrupts DNA binding (35).

Our H/DX studies of three frequent RTT mutants indicate that MBD mutations that each cause RTT in a physiological context can do so in a manner that either disrupts or preserves the inflexibility of the folded state of the MBD. Final structures are useful in predicting the local and global effects of mutation of amino acid sequences, and our H/DX studies of the MBD mutant proteins illustrates the further utility of site-resolved dynamic protein measurements to determine the extent to which point mutations affect backbone dynamics. Our studies of the F155S and T158M mutations also raise the tantalizing prospect that a subset of MBD-localized RTT mutations may benefit by so-called small molecule chaperones to return the MBD to the relative stability of the WT protein, and we propose that RTT should be added to the growing list of diseases where such pharmacological stabilization of mutant disease causing gene products (55) is pursued as a viable therapeutic approach.

Acknowledgments—We thank C. L. Woodcock for the gift of reagents and D. Stranz for kindly providing DXMS software. We also thank S. W. Englander and L. Mayne for many helpful discussions throughout these experiments and S. D'Arcy for comments on the manuscript.

REFERENCES

1. Lewis, J. D., Meehan, R. R., Henzel, W. J., Maurer-Fogy, I., Jeppesen, P., Klein, F., and Bird, A. (1992) *Cell* **69,** 905–914
2. Nan, X., Meehan, R. R., and Bird, A. (1993) *Nucleic Acids Res.* **21,** 4886–4892
3. Skene, P. J., Illingworth, R. S., Webb, S., Kerr, A. R., James, K. D., Turner, D. J., Andrews, R., and Bird, A. P. (2010) *Mol. Cell* **37,** 457–468
4. Nikitina, T., Shi, X., Ghosh, R. P., Horowitz-Scherer, R. A., Hansen, J. C., and Woodcock, C. L. (2007) *Mol. Cell. Biol.* **27,** 864–877
5. Ghosh, R. P., Horowitz-Scherer, R. A., Nikitina, T., Shlyakhtenko, L. S., and Woodcock, C. L. (2010) *Mol. Cell. Biol.* **30,** 4656–4670
6. Fraga, M. F., Ballestar, E., Montoya, G., Taysavang, P., Wade, P. A., and Esteller, M. (2003) *Nucleic Acids Res.* **31,** 1765–1774
7. Hansen, J. C., Ghosh, R. P., and Woodcock, C. L. (2010) *IUBMB Life* **62,** 732–738
8. Georgel, P. T., Horowitz-Scherer, R. A., Adkins, N., Woodcock, C. L., Wade, P. A., and Hansen, J. C. (2003) *J. Biol. Chem.* **278,** 32181–32188
9. Nikitina, T., Ghosh, R. P., Horowitz-Scherer, R. A., Hansen, J. C., Grigoryev, S. A., and Woodcock, C. L. (2007) *J. Biol. Chem.* **282,** 28237–28245
10. Jeffery, L., and Nakielny, S. (2004) *J. Biol. Chem.* **279,** 49479–49487
11. Nan, X., Ng, H. H., Johnson, C. A., Laherty, C. D., Turner, B. M., Eisenman, R. N., and Bird, A. (1998) *Nature* **393,** 386–389

12. Fuks, F., Hurd, P. J., Wolf, D., Nan, X., Bird, A. P., and Kouzarides, T. (2003) *J. Biol. Chem.* **278,** 4035–4040
13. Agarwal, N., Hardt, T., Brero, A., Nowak, D., Rothbauer, U., Becker, A., Leonhardt, H., and Cardoso, M. C. (2007) *Nucleic Acids Res.* **35,** 5402–5408
14. Kimura, H., and Shiota, K. (2003) *J. Biol. Chem.* **278,** 4806–4812
15. Kokura, K., Kaul, S. C., Wadhwa, R., Nomura, T., Khan, M. M., Shinagawa, T., Yasukawa, T., Colmenares, C., and Ishii, S. (2001) *J. Biol. Chem.* **276,** 34115–34121
16. Suzuki, M., Yamada, T., Kihara-Negishi, F., Sakurai, T., and Oikawa, T. (2003) *Oncogene* **22,** 8688–8698
17. Harikrishnan, K. N., Chow, M. Z., Baker, E. K., Pal, S., Bassal, S., Brasacchio, D., Wang, L., Craig, J. M., Jones, P. L., Sif, S., and El-Osta, A. (2005) *Nat. Genet.* **37,** 254–264
18. Nan, X., Hou, J., Maclean, A., Nasir, J., Lafuente, M. J., Shu, X., Kriaucionis, S., and Bird, A. (2007) *Proc. Natl. Acad. Sci. U.S.A.* **104,** 2709–2714
19. Chahrour, M., Jung, S. Y., Shaw, C., Zhou, X., Wong, S. T., Qin, J., and Zoghbi, H. Y. (2008) *Science* **320,** 1224–1229
20. Young, J. I., Hong, E. P., Castle, J. C., Crespo-Barreto, J., Bowman, A. B., Rose, M. F., Kang, D., Richman, R., Johnson, J. M., Berget, S., and Zoghbi, H. Y. (2005) *Proc. Natl. Acad. Sci. U.S.A.* **102,** 17551–17558
21. Yasui, D. H., Peddada, S., Bieda, M. C., Vallero, R. O., Hogart, A., Nagarajan, R. P., Thatcher, K. N., Farnham, P. J., and Lasalle, J. M. (2007) *Proc. Natl. Acad. Sci. U.S.A.* **104,** 19416–19421
22. Hite, K. C., Adams, V. H., and Hansen, J. C. (2009) *Biochem. Cell Biol.* **87,** 219–227
23. Amir, R. E., Van den Veyver, I. B., Wan, M., Tran, C. Q., Francke, U., and Zoghbi, H. Y. (1999) *Nat. Genet.* **23,** 185–188
24. Bienvenu, T., and Chelly, J. (2006) *Nat. Rev. Genet.* **7,** 415–426
25. LaSalle, J. M., Hogart, A., and Thatcher, K. N. (2005) *Int. Rev. Neurobiol.* **71,** 131–165
26. Moretti, P., and Zoghbi, H. Y. (2006) *Curr. Opin. Genet. Dev.* **16,** 276–281
27. Ballestar, E., and Esteller, M. (2005) *Biochem. Cell Biol.* **83,** 374–384
28. Bernard, D., Gil, J., Dumont, P., Rizzo, S., Monté, D., Quatannens, B., Hudson, D., Visakorpi, T., Fuks, F., and de Launoit, Y. (2006) *Oncogene* **25,** 1358–1366
29. Tompa, P. (2009) *Structure and Function of Intrinsically Disordered Proteins*, CRC Press, Boca Raton, FL
30. Dunker, A. K., Silman, I., Uversky, V. N., and Sussman, J. L. (2008) *Curr. Opin. Struct. Biol.* **18,** 756–764
31. Dunker, A. K., Brown, C. J., Lawson, J. D., Iakoucheva, L. M., and Obradović, Z. (2002) *Biochemistry* **41,** 6573–6582
32. Dyson, H. J., and Wright, P. E. (2005) *Nat. Rev. Mol. Cell Biol.* **6,** 197–208
33. Hansen, J. C., Lu, X., Ross, E. D., and Woody, R. W. (2006) *J. Biol. Chem.* **281,** 1853–1856
34. Adams, V. H., McBryant, S. J., Wade, P. A., Woodcock, C. L., and Hansen, J. C. (2007) *J. Biol. Chem.* **282,** 15057–15064
35. Ghosh, R. P., Horowitz-Scherer, R. A., Nikitina, T., Gierasch, L. M., and Woodcock, C. L. (2008) *J. Biol. Chem.* **283,** 20523–20534
36. Wakefield, R. I., Smith, B. O., Nan, X., Free, A., Soteriou, A., Uhrin, D., Bird, A. P., and Barlow, P. N. (1999) *J. Mol. Biol.* **291,** 1055–1065
37. Ho, K. L., McNae, I. W., Schmiedeberg, L., Klose, R. J., Bird, A. P., and Walkinshaw, M. D. (2008) *Mol. Cell* **29,** 525–531
38. Del Mar, C., Greenbaum, E. A., Mayne, L., Englander, S. W., and Woods, V. L., Jr. (2005) *Proc. Natl. Acad. Sci. U.S.A.* **102,** 15477–15482
39. Englander, S. W. (2006) *J. Am. Soc. Mass Spectrom.* **17,** 1481–1489
40. Chong, S., Montello, G. E., Zhang, A., Cantor, E. J., Liao, W., Xu, M. Q., and Benner, J. (1998) *Nucleic Acids Res.* **26,** 5109–5115
41. Black, B. E., Foltz, D. R., Chakravarthy, S., Luger, K., Woods, V. L., Jr., and Cleveland, D. W. (2004) *Nature* **430,** 578–582
42. Black, B. E., Brock, M. A., Bédard, S., Woods, V. L., Jr., and Cleveland, D. W. (2007) *Proc. Natl. Acad. Sci. U.S.A.* **104,** 5008–5013
43. Hamuro, Y., Wong, L., Shaffer, J., Kim, J. S., Stranz, D. D., Jennings, P. A., Woods, V. L., Jr., and Adams, J. A. (2002) *J. Mol. Biol.* **323,** 871–881
44. Coales, S. J., E. S. Y., Lee, J. E., Ma, A., Morrow, J. A., and Hamuro, Y. (2010) *Rapid Commun. Mass Spectrom.* **24,** 3585–3592
45. Pantazatos, D., Kim, J. S., Klock, H. E., Stevens, R. C., Wilson, I. A., Lesley, S. A., and Woods, V. L., Jr. (2004) *Proc. Natl. Acad. Sci. U.S.A.* **101,** 751–756
46. Sekulic, N., Bassett, E. A., Rogers, D. J., and Black, B. E. (2010) *Nature* **467,** 347–351
47. Ghosh, R. P., Nikitina, T., Horowitz-Scherer, R. A., Gierasch, L. M., Uversky, V. N., Hite, K., Hansen, J. C., and Woodcock, C. L. (2010) *Biochemistry* **49,** 4395–4410
48. Wright, P. E., and Dyson, H. J. (2009) *Curr. Opin. Struct. Biol* **19,** 31–38
49. Fuxreiter, M., Tompa, P., Simon, I., Uversky, V. N., Hansen, J. C., and Asturias, F. J. (2008) *Nat. Chem. Biol.* **4,** 728–737
50. Lin, S., and Riggs, A. D. (1975) *Cell* **4,** 107–111
51. Kalodimos, C. G., Biris, N., Bonvin, A. M., Levandoski, M. M., Guennuegues, M., Boelens, R., and Kaptein, R. (2004) *Science* **305,** 386–389
52. Lewis, M., Chang, G., Horton, N. C., Kercher, M. A., Pace, H. C., Schumacher, M. A., Brennan, R. G., and Lu, P. (1996) *Science* **271,** 1247–1254
53. Kumar, A., Kamboj, S., Malone, B. M., Kudo, S., Twiss, J. L., Czymmek, K. J., LaSalle, J. M., and Schanen, N. C. (2008) *J. Cell Sci.* **121,** 1128–1137
54. Yang, C., van der Woerd, M. J., Muthurajan, U. M., Hansen, J. C., and Luger, K. (2011) *Nucleic Acids Res.*, in press
55. Ringe, D., and Petsko, G. A. (2009) *J. Biol.* **8,** 80